RL-TR-94-100
Final Technical Report
August 1994

ALTERNATIVE VOLUME INTEGRAL EQUATION FORMULATIONS APPLIED TO DIELECTRIC CYLINDERS

SRI International

Rose W. Wang

APPROVED FOR PUBLIC RELEASE; DISTRIBUTION UNLIMITED.

Rome Laboratory
Air Force Materiel Command
Griffiss Air Force Base, New York

This report has been reviewed by the Rome Laboratory Public Affairs Office (PA) and is releasable to the National Technical Information Service (NTIS). At NTIS it will be releasable to the general public, including foreign nations.

RL-TR-94-100 has been reviewed and is approved for publication.

APPROVED:

Arthur D. Yaghjian

ARTHUR D. YAGHJIAN
Project Engineer

FOR THE COMMANDER

Robert V. McGahan

ROBERT V. McGAHAN
Acting Director
Electromagnetics & Reliability Directorate

If your address has changed or if you wish to be removed from the Rome Laboratory mailing list, or if the addressee is no longer employed by your organization, please notify RL (ERCT) Hanscom AFB MA 01731. This will assist us in maintaining a current mailing list.

Do not return copies of this report unless contractual obligations or notices on a specific document require that it be returned.

REPORT DOCUMENTATION PAGE

Form Approved
OMB No. 0704-0188

1. AGENCY USE ONLY (Leave Blank)	2. REPORT DATE	3. REPORT TYPE AND DATES COVERED
	August 1994	Final Sep 92 - Sep 93

4. TITLE AND SUBTITLE
ALTERNATIVE VOLUME INTEGRAL EQUATION FORMULATIONS APPLIED TO DIELECTRIC CYLINDERS

5. FUNDING NUMBERS
C - F30602-91-D-0001
Task E-2-7160, 15
PE - 61102F
PR - 2304
TA - I4
WU - P1

6. AUTHOR(S)
Rose W. Wang

7. PERFORMING ORGANIZATION NAME(S) AND ADDRESS(ES)
SRI International
333 Ravenswood Avenue
Menlo Park, San Mateo County, CA 94025

8. PERFORMING ORGANIZATION REPORT NUMBER
N/A

9. SPONSORING/MONITORING AGENCY NAME(S) AND ADDRESS(ES)
Rome Laboratory (ERCT)
31 Grenier Street
Hanscom AFB MA 01731-3010

10. SPONSORING/MONITORING AGENCY REPORT NUMBER
RL-TR-94-100

11. SUPPLEMENTARY NOTES
Rome Laboratory Project Engineer: Arthur D. Yaghjian/ERCT/(617) 377-3961

12a. DISTRIBUTION/AVAILABILITY STATEMENT
Approved for public release; distribution unlimited.

12b. DISTRIBUTION CODE

13. ABSTRACT (Maximum 200 words)

A new volume-surface integral equation method is used for evaluating the bistatic scattering from dielectric cylinders with high dielectric constants. The kernel of this alternate volume-surface integral equation is less singular than the original volume integral equation because it does not require the computation of the double derivative $(\nabla\nabla\psi)$ in the highly singular dyadic Green's function. Numerical results indicate that there is a significant improvement in performance by using this new volume-surface integral formulation. We can achieve better accuracy, and require fewer cells per wavelength in the computations than with the original volume integral equation.

14. SUBJECT TERMS
Volume-Surface Integral Equations, Penetrable Bodies, Bistatic Scattering, Dielectric Cylinders

15. NUMBER OF PAGES
56

16. PRICE CODE

17. SECURITY CLASSIFICATION OF REPORT	18. SECURITY CLASSIFICATION OF THIS PAGE	19. SECURITY CLASSIFICATION OF ABSTRACT	20. LIMITATION OF ABSTRACT
UNCLASSIFIED	UNCLASSIFIED	UNCLASSIFIED	UL

TABLE OF CONTENTS

1. INTRODUCTION

One of the standard approaches for calculating electromagnetic scattering from inhomogeneous bodies involves using the method of moments applied to the volume integral equation [1]-[3]. During the past decades, numerous researchers have been unsuccessful in their efforts to obtain an accurate solution, in particular, for problems that involve large bodies with large dielectric constants. In recent years, some researchers have been able to obtain an accurate solution with somewhat sophisticated basis functions - such as rooftop, tetrahedral and polygonal functions [4]-[7] - instead of the traditional simple pulse basis functions. However, the program becomes more complex and the number of cells required per wavelength remains large.

In this report, we propose an alternative formulation for the volume integral equation [8]. This new formulation involves both the volume and surface integrals but unlike Jin, Liepa and Tai's volume-surface integral equation [9], it is applicable to three dimensional problems. There is no double derivative operating on the kernel inside this new volume-surface integral equation so that it is less singular than the volume integral equation. In addition, it can be solved using simple pulse basis functions and point matching. Numerically, it is more efficient than the original volume integral equation [10]-[11].

We began the task by applying the newly derived volume-surface integral equation to the computation of electromagnetic scattering from dielectric cylinders. We formulated the new volume-surface integral equation numerically, and tested the validity of the new computer code by comparing with the results of both the original volume integral equation and a surface integral equation.

Initially, the volume-surface integral equation was discretized as follows. The volume integral was divided into small square cells (in the case of cylinder) with the equivalent current assumed constant throughout each cell. The surface integral in the equation was divided into small segments with the current assumed constant within each segment. When a segment was also part of a cell, the current was assumed to be the same in the cell as well as in the segment. However, this procedure produced inaccurate results. We then allowed the currents in the cells and in the segment to have independent values. This numerical scheme proved more accurate for the bistatic scattering from square cylinders. Point matching was used throughout.

Our next step involved the special treatment of the bordering cells. Specifically, when the source point is in the cell and the observation points are in the bordering segment within the same cell, the Green's function in the volume integral term was integrated analytically. In addition, we integrated the volume integral term for all the cells quite precisely. Instead of approximating the Green's function by its value at the center of each cell, we integrated the Green's function accurately by converting the volume integral into a surface integral over each cell. With this special treatment of the bordering cells and the accurate integration of the volume integral terms, we hoped to achieve higher accuracy. We then compared the computed bistatic scattering for the dielectric square cylinder to that obtained from the surface integral method by using the program CICERO from McDonnell Douglas Corporation. Results indicated that there is negligible difference in performance between using this more sophisticated numerical treatment and the volume-surface integral equation method with no treatment (see Fig. 1). The two methods agreed favorably with the results of the CICERO program for all frequencies.

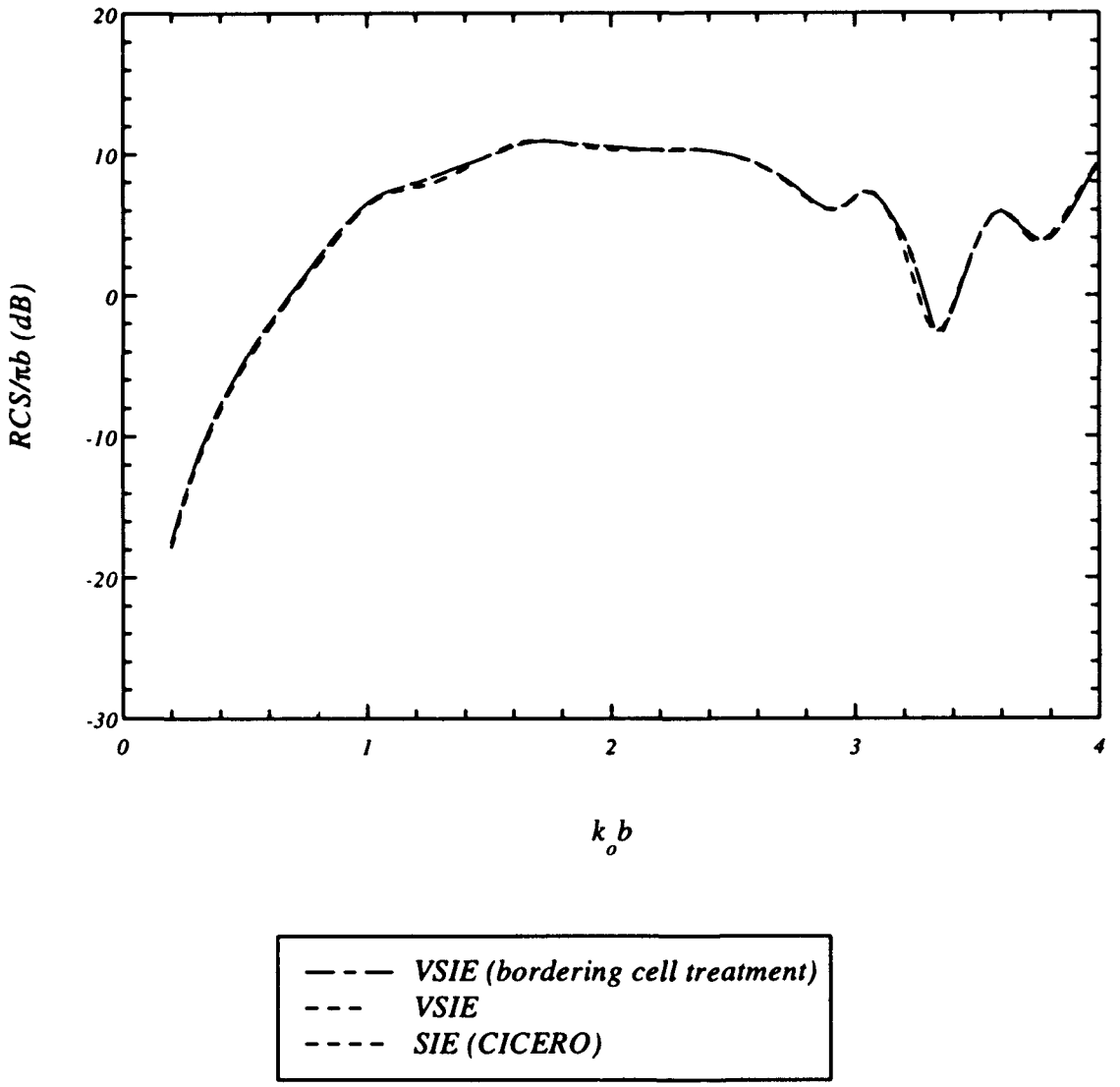

Fig. 1 Forward scattering from a dielectric square cylinder with relative permittivity $\varepsilon_r = 4$, $n/\lambda_d = 10$, TE polarization.

To test the validity of the new volume-surface integral equation program, extensive numerical experimentation was done. As a preliminary step, we compared our computed bistatic scattering for the dielectric lossy square cylinder with the scattering computed from the CICERO program for different relative permittivities and cylinder sizes. Unlike the initial volume integral equation, this alternate equation gave results that coincided with those of the CICERO program. These consistent results indicate that the new volume-surface integral equation performs much better than the original volume integral equation.

Our final test involved the computation of scattering from dielectric cylinders with large relative permittivity. We solved our volume-surface integral equation for the case of the square cylinder with a complex relative permittivity ($\varepsilon_r = 72 + i161.85248$) in order to compare with the results of Borup, Sullivan and Gandhi [12], who used the traditional volume integral equation. Our results attained greater accuracy with 12 cells per dielectric wavelength than Gandhi's method with 28 cells per dielectric wavelength. The wavelength in the dielectric was computed as $\lambda_o/\sqrt{|\varepsilon_r|}$. Unfortunately, the results indicated that there is still about a 2 dB difference for forward and back scattering from square cylinders when compared with the surface integral equation method (see Fig. 14).

The transverse currents (J_x and J_y) along the edges change very rapidly. We thought that this may be an indication that our assumption of constant current along the segments is not a good approximation. We tried the revised approach of using a linear approximation for currents along the segments, and integrating along the transverse self-segment more accurately. Nevertheless, even with this more accurate formulation, the results remained the same.

One of the more important factors that influence the original volume integral equation is the edge current effect for high dielectric, small bodies. Consider the case of electromagnetic scattering from a small rectangular dielectric cylinder of relative permittivity $\varepsilon_r = 72$, and $k_o b = \pi/10$ (k_o is the free space wave number, and b is one half side length of the square cylinder). Our results show that the currents near the edges change very rapidly. Even if the cylinder's size may be small, the rapid changes of the currents around the edges cannot be detected unless we use very fine cell sizes on the order of $n/\lambda_d = 30$, where n/λ_d is the number of cells per dielectric wavelength. The coarse discretization of the edge currents may be the reason why there is a 2 dB difference in Fig. 14 between the results of the new volume-surface integral equation and the results of the surface integral equation. In order to minimize the dimension of the cells, our new scheme involves maintaining the same cell size throughout the center of the body while discretizing the cells more finely near the edges for small bodies with high dielectric constants. This procedure produced higher accuracy than the volume-surface integral equation without finer discretization near the boundary cells. With finer discretization near the border of the scatterer, much fewer cells per wavelength were needed overall to achieve much greater accuracy than with the original volume integral equation (using pulse basis functions and point matching).

2. VOLUME-SURFACE INTEGRAL EQUATION

2.1 Three-Dimensional Volume-Surface Integral Equation

Consider electromagnetic wave scattering from an inhomogeneous scatterer with complex relative permittivity ε_r (see Fig. 2). The electric-field volume integral equation can be written in the form [13]

$$\boldsymbol{E}^{inc}(\boldsymbol{r}) = \boldsymbol{E}^{total}(\boldsymbol{r}) + \frac{k_o^2}{i\omega\varepsilon_o} \lim_{\delta \to 0} \iiint_{V-V_\delta} \boldsymbol{J}(\boldsymbol{r}') \cdot \bar{G}_e(\boldsymbol{r},\boldsymbol{r}')dv' - \frac{\bar{L}_\delta \cdot \boldsymbol{J}(\boldsymbol{r})}{i\omega\varepsilon_o} \qquad (1)$$

where

$$\boldsymbol{J} = \tau \boldsymbol{E}^{total} = [\sigma - i\omega(\varepsilon - \varepsilon_o)]\boldsymbol{E}^{total} \qquad (2)$$

$$\bar{G}_e = \left(\frac{\nabla'\nabla'}{k_o^2} + \bar{I}\right)\frac{e^{ik_o|r-r'|}}{4\pi|r-r'|} \qquad (3)$$

$$k_o = \omega\sqrt{\mu_o\varepsilon_o} \qquad \text{wave number in free space} \qquad (4)$$

$$\omega = 2\pi f \qquad \text{angular frequency.} \qquad (5)$$

The permittivity in free space is denoted as ε_o. $\boldsymbol{r}$ and $\boldsymbol{r}'$ are the source and observation position vectors. $\bar{I}$ is the unit dyadic and $\bar{L}_\delta$ is the source dyadic which depends on the geometry of the principal volume V_δ which becomes infinitesimally small as the chord length δ approaches zero, and finally, V denotes the volume of the scatterer.

The procedure in this formulation is based on volume discretizations of the volume integral equation with pulse basis functions and point matching. However, for 3-D problems as well as 2-D problems for TE polarization of bistatic scattering from high dielectric bodies, substantial inaccuracies are observed. Recently, Zwamborn and van den Berg [14]-[15] have been successful in obtaining an accurate solution using different testing and expansion functions instead of the simpler basis functions. However, the program becomes more complex and the number of cells required remains large.

Volume-surface integral equations for inhomogeneous cylinders were first presented by Jin, Liepa and Tai. In their paper, they were successful in obtaining an accurate solution using simple pulse basis functions and point matching. However, their formulation cannot be applied to three dimensional problems. Recently, Wust et al. [16] have developed a new volume-surface integral equation for the calculation of 3-dimensional electromagnetic fields problems. However, their formulation is not applicable to continuously varying inhomogeneous bodies or to observation points that approach the surface. For these reasons, we develop an alternative volume-surface integral equation for three dimensional inhomogeneous bodies.

Let us begin with an alternative form of the volume-surface integral equation

$$E^{inc}(r) = E^{total} + \frac{1}{i\omega\varepsilon_o}\iiint_V \left[k_o^2 J(r')\psi(r,r') - \nabla' \cdot J(r')\nabla'\psi(r,r')\right]dv'. \quad (6)$$

By using the relation between the divergence of the polarization current and the gradient of the relative permittivity as derived in [8],

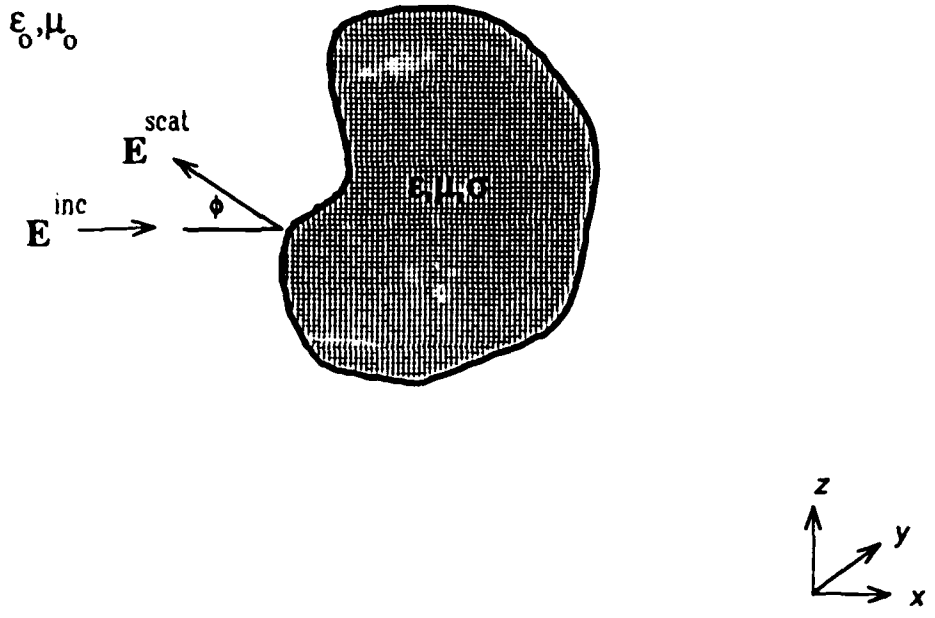

Fig. 2 Electromagnetic scattering from a dielectric body.

$$\nabla \cdot J(r) = -\frac{i\omega\varepsilon_o}{\tau}\frac{\nabla\varepsilon_r}{\varepsilon_r}\cdot J(r) \tag{7}$$

and by evaluating both the volume integral and the surface integral just inside the dielectric interface of the body, a new formulation of the volume-surface integral equation is obtained:

$$E^{inc}(r) = \frac{J(r)}{\tau} + \frac{1}{i\omega\varepsilon_o}\iiint_{V^-}[k_o^2 J(r')\psi(r,r') + \frac{i\omega\varepsilon_o}{\tau}\frac{\nabla'\varepsilon_r}{\varepsilon_r}\cdot J(r')\nabla'\psi(r,r')]dv'$$

$$+\frac{1}{i\omega\varepsilon_o}\iint_{s^-}\hat{n}\cdot J(r')\nabla'\psi(r,r')ds' \tag{8}$$

$$\psi(r,r') = \frac{e^{ik_o|r-r'|}}{4\pi|r-r'|} \quad \text{for three dimensions} \tag{9}$$

where ε_r is the relative permittivity of the body, and $\hat{n}$ is the unit normal. V^- and s^- denotes the volume and surface just inside the dielectric interface.

The application of the method of moments to Eq. 8 involves evaluating both the volume integral and the surface integrals just inside the dielectric interface of the body. Using pulse basis functions and point matching, the source and observation points are chosen to be inside the volume as well on the surface just inside the dielectric interface. However, by letting the observation point approach the surface from the inside of the dielectric, the surface integral in the volume-surface integral equation can be computed very accurately [17] by transforming it into a surface principal value integral of Eq. 10. The last term of this integral equation is the term that arises by letting the observation point approach the source point in the surface integral. Eq. 8 is valid for both the observation point inside

the volume and as the observation point approaches the surface. However, Eq. 10 is valid and preferable to Eq. 8 for an observation point on the surface.

$$E^{inc}(r)=\frac{J(r)}{\tau}+\frac{1}{i\omega\varepsilon_o}\iiint_{V^-}\left[k_o^2 J(r')\psi(r,r')+\frac{i\omega\varepsilon_o}{\tau}\frac{\nabla'\varepsilon_r}{\varepsilon_r}\cdot J(r')\nabla'\psi(r.r')\right]dv'$$
$$+\frac{1}{i\omega\varepsilon_o}\oiint_{S^-}\hat{n}\cdot J(r')\nabla'\psi(r,r')ds'-\frac{J_n(r)\hat{n}}{2i\omega\varepsilon_o}. \qquad (10)$$

The kernels of these new volume-surface integral equations are less singular than the original integral equation because they do not require the computation of the double derivative ($\nabla\nabla\psi$) in the highly singular dyadic Green's function of the original equation (Eq. 1). Moreover, when applying the MOM with pulse basis functions and point matching to the original volume integral equation, as discussed by Peterson [18], the treatment of surface charge densities is not properly addressed, and as a result, fictitious charge layers are present at every cell boundary leading to inaccurate results. Our new volume-surface integral equations involve only the scalar free-space Green's function and its gradient which are less singular than the dyadic Green's function of the original volume-surface integral equation (Eq. 1). It, therefore, does not encounter these fictitious charge layers.

2.2 Two-Dimensional Volume-Surface Integral Equation

For two dimensional problems, the volume-surface integral equation has the same form, except the volume integral becomes a surface integral and the surface integral becomes a line integral. In addition, the free space Green's function now becomes a Hankel function. The two-dimensional form of the volume-surface integral equation corresponding to Eq.(8) can be written as

$$E^{inc}(t) = \frac{J(t)}{\tau} + \frac{1}{i\omega\varepsilon_o}\iint_{s-} k_o^2 J(t')\psi(t,t')ds'$$

$$+\iint_{s-} \frac{\nabla'\varepsilon_r}{\varepsilon_r}\cdot\frac{J(t')}{\tau}\nabla'\psi(t,t')ds'$$

$$+\frac{1}{i\omega\varepsilon_o}\int_{c-}\hat{n}\cdot J(t')\nabla'\psi(t,t')dt'. \qquad (11)$$

Similarly, for observation points approaching the dielectric boundary, from the inside of the scatterers, Eq. 11 becomes

$$E^{inc}(t) = \frac{J(t)}{\tau} + \frac{1}{i\omega\varepsilon_o}\iint_{s-} k_o^2 J(t')\psi(t,t')ds'$$

$$+\iint_{s-} \frac{\nabla'\varepsilon_r}{\varepsilon_r}\cdot\frac{J(t')}{\tau}\nabla'\psi(t,t')ds'$$

$$+\frac{1}{i\omega\varepsilon_o}\oint_{c-}\hat{n}\cdot J(t')\nabla'\psi(t,t')dt' - \frac{J_n(t)\hat{n}}{2i\omega\varepsilon_o} \qquad (12)$$

where

$$\psi(t,t') = \frac{i}{4}H_o^{(1)}(k_o|t-t'|) \text{ for two dimensions} \qquad (13)$$

and $H_0^{(1)}$ is the zeroth order Hankel function of the first kind, t and t' are the source and observation position vectors for two dimensional problems.

For homogeneous cylinders, the third term on the right side of Eq. 11 vanishes and it simplifies to

$$E^{inc}(t) = \frac{J(t)}{\tau} + \frac{\omega\mu_o}{4}\iint_{s-} J(t')H_o^{(1)}(t,t')ds'$$

$$+\frac{1}{4\omega\varepsilon_o}\int_{c^-} \hat{n}\cdot J(t')\nabla' H_o^{(1)}(k_o|t-t'|)dt'. \qquad (14)$$

Similarly, for homogeneous cylinders, the third term on the right side of Eq. 12 vanishes, and we have

$$E^{inc}(t) = \frac{J(t)}{\tau} + \frac{\omega\mu_o}{4}\iint_{s-} J(t')H_o^{(1)}(t,t')ds'$$

$$+\frac{1}{4\omega\varepsilon_o}\oint_{c^-} \hat{n}\cdot J(t')\nabla' H_o^{(1)}(k_o|t-t'|)dt'$$

$$-\frac{(\hat{n}\cdot J(t))\hat{n}}{2i\omega\varepsilon_o}. \qquad (15)$$

Using Eqs. (14)-(15), we are able to compute the bistatic scattering problems for two-dimensional homogeneous problems using pulse basis functions and point matching. Eqs. (11)-(12) and Eqs.(14)-(15) are valid for both TE and TM polarizations. In the TM case, the current density J has only a z component and thus the $\hat{n}\cdot J$ terms all disappear in these equations leaving a TM equation identical to the original TM volume integral equation. An additional line integral in Eqs. (11)-(12) and Eqs. (14)-(15) replaces the highly singular part of the original volume integral equation making this new volume-surface integral equation much better conditioned.

2.3 Scattering from Dielectric Cylinders

In applying the MOM to the volume-surface integral equation using simple pulse basis functions and point matching, we assumed that both the electric field and the dielectric properties are constant in each cell. Commonly, the Green's function is evaluated at the center of each cell. In other words, there is one center point for each non-self cell calculation.

For two-dimensional electromagnetic scattering from dielectric cylinders, we divided the cylinder into small square cells for the surface and small line segments for the edges. Currents are assumed to be constant within each cell as well as within each segment. Both the currents in the cells as well as in the segments are assumed to have independent values even though the segments are also part of the cells.

Consider the problem of scattering from a square dielectric cylinder (Fig. 3). The square dielectric cylinder is divided into equal size square cells with the bordering segment the same length as the length of each cell. Suppose the dielectric square cylinder is illuminated by a time-harmonic electromagnetic field with time dependence $e^{-i\omega t}$. Using the pulse basis functions and point matching method, the incident field for observation points in the surface becomes

$$E^{inc}(t_i) = \frac{J(t_i)}{\tau} + \frac{\omega\mu_o}{4} \sum_{j=1, j\neq i}^{N} J(t_j) H_o^{(1)}(k_o|(t_i - t_j|)\Delta s$$

$$+ \frac{\omega\mu_o}{4} J(t_i) \frac{2H_1^{(1)}(k_o r'')}{k_o r''} \Delta s + \frac{i}{\omega\varepsilon_o} J(t_i)$$

$$+ \frac{1}{4\omega\varepsilon_o} \sum_{l=1}^{M} \hat{n} \cdot J(t_l) \nabla' H_o^{(1)}(k_o|(t_i - t_l|)\Delta l \qquad (16)$$

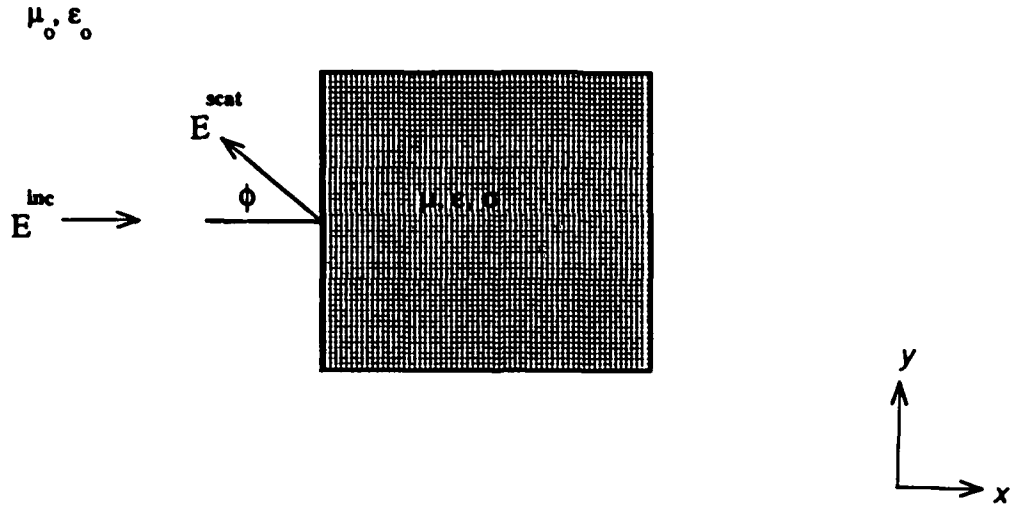

Fig. 3 Scattering from dielectric square cylinder.

where $r'' = \sqrt{\frac{\Delta s}{\pi}}$. (17)

Δs denotes the area of the cells, and Δl denotes the length of the segment of the body. The subscripts i, j and l denote the observation point, the source point in the cell and the source point in the segment, respectively.

For observation points on the boundary we have

$$E^{inc}(t_i) = \frac{J(t_i)}{\tau} + \frac{\omega\mu_o}{4}\sum_{j=1}^{N} J(t_j) H_o^{(1)}(k_o|(t_i - t_j|)\Delta s$$

$$+\frac{1}{4\omega\varepsilon_o}\sum_{l=1,l\neq i}^{M} \hat{n}\cdot J(t_l)\nabla' H_o^{(1)}(k_o|(t_i - t_l|)\Delta l$$

$$-\frac{\hat{n}\cdot J(t_i)\hat{n}}{2i\omega\varepsilon_o}. \quad (18)$$

The x component of the incident field when the observation point is in the surface is given by

$$E_x^{inc}(t_i) = \frac{J_x(t_i)}{\tau} + \frac{\omega\mu_o}{4}\sum_{j=1,j\neq i}^{N} J_x(t_j) H_o^{(1)}(k_o|(t_i - t_j|)\Delta s$$

$$+\frac{\omega\mu_o}{4} J_x(t_i)\frac{2H_1^{(1)}(k_o r'')}{k_o r''}\Delta s + \frac{i}{\omega\varepsilon_o} J_x(t_i)$$

$$+\frac{\omega\mu_o}{4k_o}\sum_{l=1}^{M} \hat{n}\cdot J(t_l)\frac{(x_i - x_l)}{|t_i - t_l|} H_1^{(1)}(k_o|(t_i - t_l|)\Delta l. \quad (19)$$

Using Eq.18, when the observation point is in the boundary, the x component of the incident field is

$$E_x^{inc}(t_i) = \frac{J_x(t_i)}{\tau} + \frac{\omega\mu_o}{4}\sum_{j=1}^{N} J_x(t_j) H_o^{(1)}(k_o|(t_i - t_j|)\Delta s$$

$$+\frac{\omega\mu_o}{4k_o}\sum_{l=1,l\neq i}^{M} \hat{n}\cdot J(t_l)\frac{(x_i - x_l)}{|t_i - t_l|} H_1^{(1)}(k_o|(t_i - t_l|)\Delta l$$

$$-\frac{\hat{n}\cdot J(t_i)(\hat{n}\cdot\hat{x})}{2i\omega\varepsilon_o}. \qquad (20)$$

Similarly, the y components of the incident fields when the observation points are in the surface and in the segment are shown in Eqs. 21 and 22 respectively.

$$E_y^{inc}(t_i) = \frac{J_y(t_i)}{\tau} + \frac{\omega\mu}{4}\sum_{j=1,j\neq i}^{N} J_y(t_j) H_o^{(1)}(k_o|(t_i - t_j|)\Delta s$$

$$+\frac{\omega\mu_o}{4} J_y(t_i)\frac{2H_1^{(1)}(k_o r'')}{k_o r''}\Delta s + \frac{i}{\omega\varepsilon_o} J_y(t_i)$$

$$+\frac{\omega\mu_o}{4k_o}\sum_{l=1}^{M} \hat{n}\cdot J(t_l)\frac{(y_i - y_l)}{|t_i - t_l|} H_1^{(1)}(k_o|(t_i - t_l|)\Delta l \qquad (21)$$

and

$$E_y^{inc}(t_i) = \frac{J_y(t_i)}{\tau} + \frac{\omega\mu_o}{4}\sum_{j=1}^{N} J_y(t_j) H_o^{(1)}(k_o|(t_i - t_j|)\Delta s$$

$$+\frac{\omega\mu_o}{4k_o}\sum_{l=1,l\neq i}^{M} \hat{n}\cdot J(t_l)\frac{(y_i - y_l)}{|t_i - t_l|} H_1^{(1)}(k_o|(t_i - t_l|)\Delta l$$

$$-\frac{\hat{n}\cdot J(t_i)(\hat{n}\cdot\hat{y})}{2i\omega\varepsilon_o}. \qquad (22)$$

This new volume-surface integral equation can be written in terms of two separate matrix equations, to evaluate the polarization current J on the surface as well as on the segment.

$$\left[E_n^{inc}\right]_{surface} = \left[Z_{nn}\right]\left[J_{nn}\right]_{surface} + \left[Z_{nm}\right]\left[J_{nm}\right]_{segment} \qquad (23)$$

$$\left[E_m^{inc}\right]_{segment} = \left[Z_{mn}\right]\left[J_{mn}\right]_{surface} + \left[Z_{mm}\right]\left[J_{mm}\right]_{segment} \qquad (24)$$

Separating the x and y components of the incident field (see Eqs. 20-22), the matrix equation can be rewritten as

$$\begin{bmatrix} E_{x_i}^{surface} \\ E_{y_{i+N}}^{surface} \\ E_{x_{i+2N}}^{segment} \\ E_{y_{i+2N+M}}^{segment} \end{bmatrix}^{inc} = \begin{bmatrix} Z_{i,j} & Z_{i,j+N} & Z_{i,j+2N} & Z_{i,j+2N+M} \\ Z_{i+N,j} & Z_{i+N,j+N} & Z_{i+N,j+2N} & Z_{i+N,j+2N+M} \\ Z_{i+2N,j} & Z_{i+2N,j+N} & Z_{i+2N,j+2N} & Z_{i+2N,j+2N+M} \\ Z_{i+2N+M,j} & Z_{i+2N+M,j+N} & Z_{i+2N+M,j+2N} & Z_{i+2N+M,j+2N+M} \end{bmatrix} \begin{bmatrix} J_{x_j}^{surface} \\ J_{y_{j+N}}^{surface} \\ J_{x_{j+2N}}^{segment} \\ J_{y_{j+2N+M}}^{segment} \end{bmatrix} \qquad (25)$$

where $n = 1, 2, ..., N$, and $m = 1, 2, ..., M$,

N = total number of cells on the surface,

M = total number of divisions on the line segment,

i = source point,

j = observation point on the body.

The evaluation of the polarization currents in the volume-surface integral equation can now be performed by solving this matrix equation using Gaussian elimination techniques.

3. NUMERICAL RESULTS

Extensive numerical experimentation was performed to determine the accuracy of this new volume-surface integral equation. The results of far field scattering from homogeneous dielectric square cylinders are compared first with the results from the original volume integral equation, and then with those obtained by a surface integral equation. The dielectric square cylinders were tested with different dielectric constants, varying sizes, and for cases when losses were present.

Fig. 4 shows the back scattering from a dielectric square cylinder versus $k_o b$ where k_o is the wave number in free space, and b is half the side of the square cylinder. The relative permittivity ε_r is 10 and the number of cells per dielectric wavelength n/λ_d is 12, for TE polarization. We set the relative permittivity to be 10 in order to examine if the revised volume-surface integral works well for large values of $k_o b$. From the figure, it can be observed that the volume integral equation curve corresponds well with the surface integral equation curve for values of $k_o b$ less than 1.7. Beyond $k_o b = 1.7$, the volume integral curve diverges from the other two curves. On the other hand, our newly formulated volume-surface integral curve matches closely with the surface integral curve for all values of $k_o b$. This preliminary result has demonstrated that the volume-surface integral equation gives improved results over the original volume integral equation for larger values of $k_o b$.

At $k_o b = 2$, the behavior of the volume integral equation is compared with that of the new volume-surface integral equation and the surface integral equation by plotting the bistatic scattering from a dielectric square cylinder of relative permittivity 10 for TE

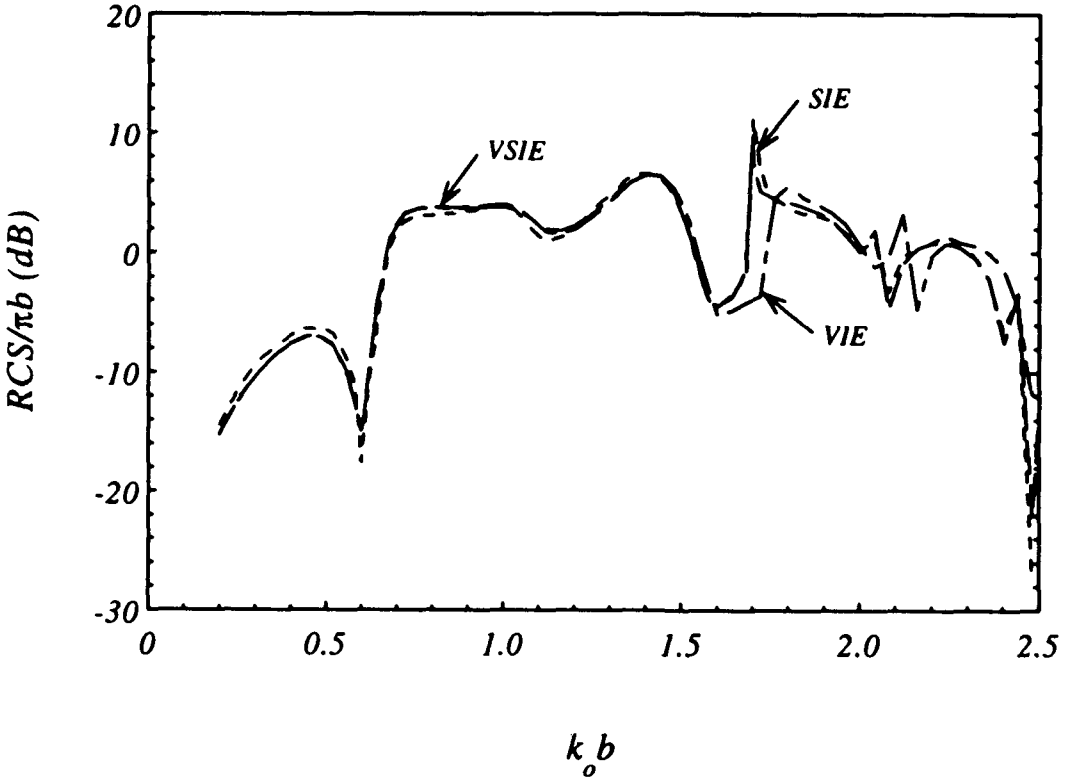

Fig. 4 Back scattering from a long dielectric square cylinder with relative permittivity $\varepsilon_r = 10$, $n/\lambda_d = 12$, TE polarization.

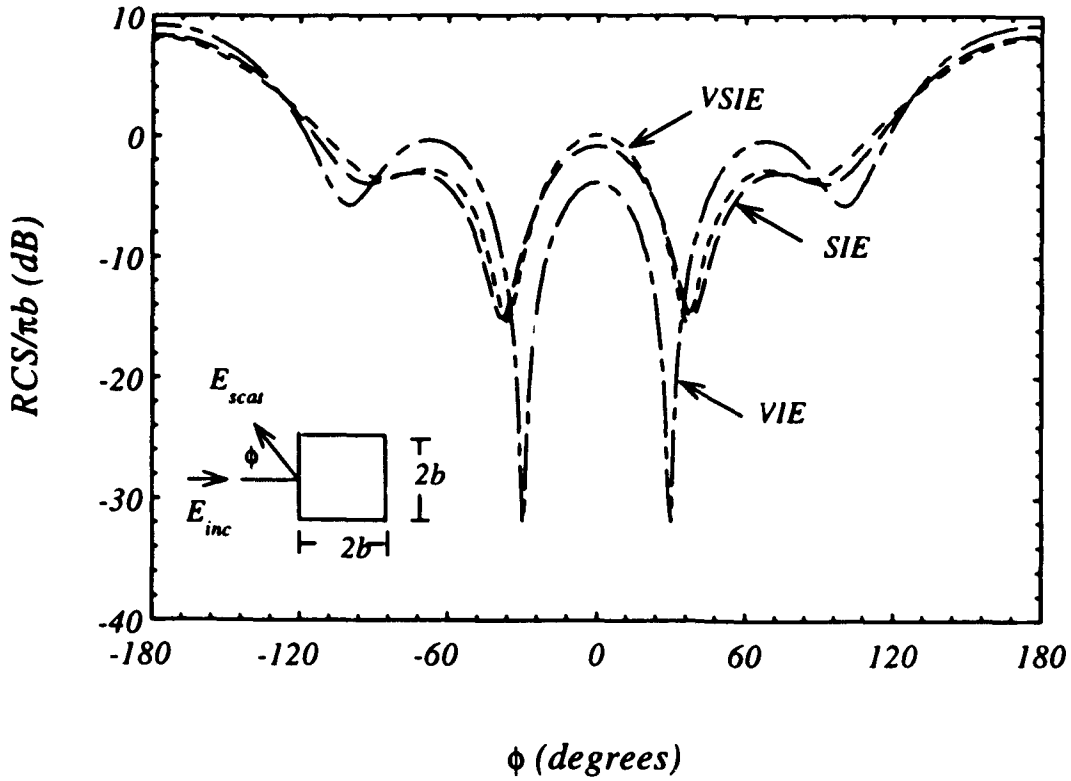

Fig. 5 Bistatic scattering from a long dielectric square cylinder with relative permittivity $\varepsilon_r = 10$, $n/\lambda_d = 12$, $k_o b = 2$, TE polarization.

polarization. Looking at Fig. 5, it is observed that even though the volume integral equation curve matched closely the two other curves at 0° back scattering, and 180° forward scattering, it is still appreciably different from the other two curves at all other angles. This confirms that the volume integral equation does not work for large values of $k_o b$. The volume-surface integral curve matched closely with the surface integral equation curve for all angles. This excellent performance is again strong indication that the volume-surface integral equation is superior to the original volume integral equation.

Our next step involved testing dielectric lossy square cylinders to ensure that the volume-surface integral equation worked for both lossless and lossy cases. Shown in Figs. 6-9 are the results of bistatic scattering from a dielectric lossy square cylinder versus the amount of loss in terms of $(i\sigma/\omega\varepsilon_o)$ for TE polarization, with the relative permittivity set to 10 and the cylinder's size $(k_o b)$ set equal to 1 and 2, respectively. The results from our revised volume-surface integral equation method compared favorably with the results of the surface integral equation method (program Cicero from McDonnell Douglas Corporation).

We also tested the validity of the volume-surface integral equation by setting the losses on the cylinder constant and varying the values of $k_o b$ which may be accomplished by either keeping the frequency constant and varying the size of the cylinder or by varying the frequency applied and keeping the size of the cylinder constant. We chose two values for the relative permittivity, $\varepsilon_r = 10 + i1.0$ and $\varepsilon_r = 10 + i2.0$, for our test. The bistatic scattering from the dielectric lossly square cylinder versus the values of $k_o b$ for TE polarization are shown in Figs 10-13. The results obtained from the volume-surface integral equation agree excellently with the curve from the surface integral equation method. The forward scattering from the dielectric lossly square cylinders is shown in Figs. 10-11, and the back scattering is shown in Figs. 12 -13.

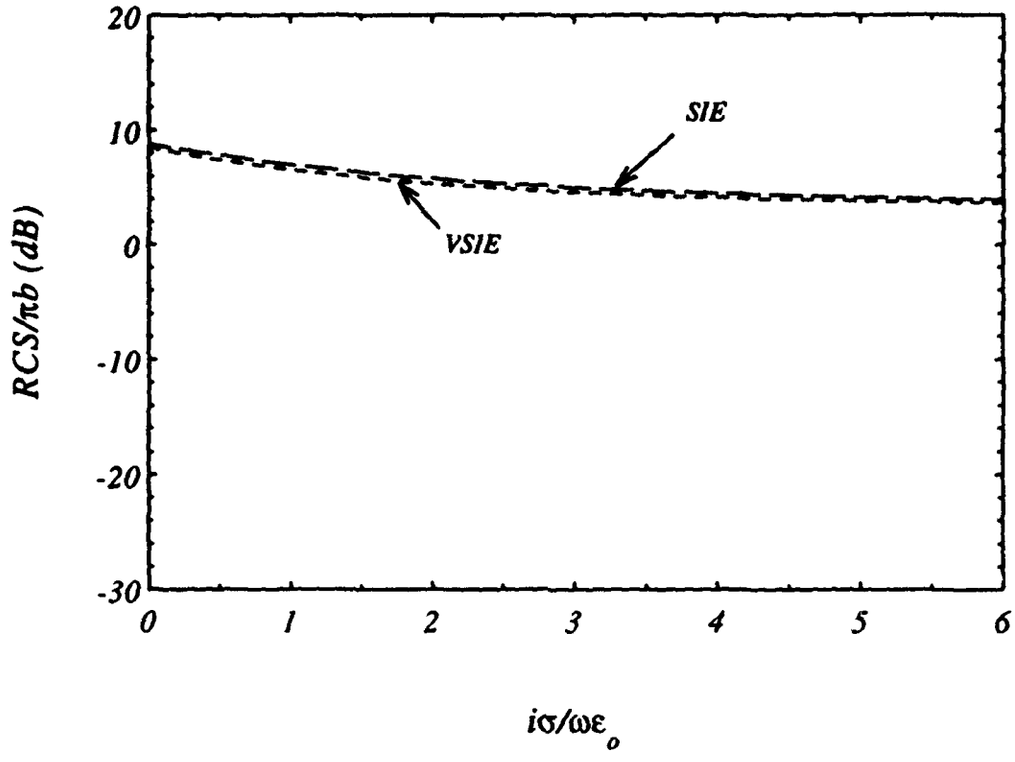

Fig. 6 Forward scattering from a long dielectric square cylinder versus $(i\sigma/\omega\varepsilon_o)$, with relative permittivity $\varepsilon_r = 10$, $k_o b = 1$, $n/\lambda_d = 12$, TE polarization.

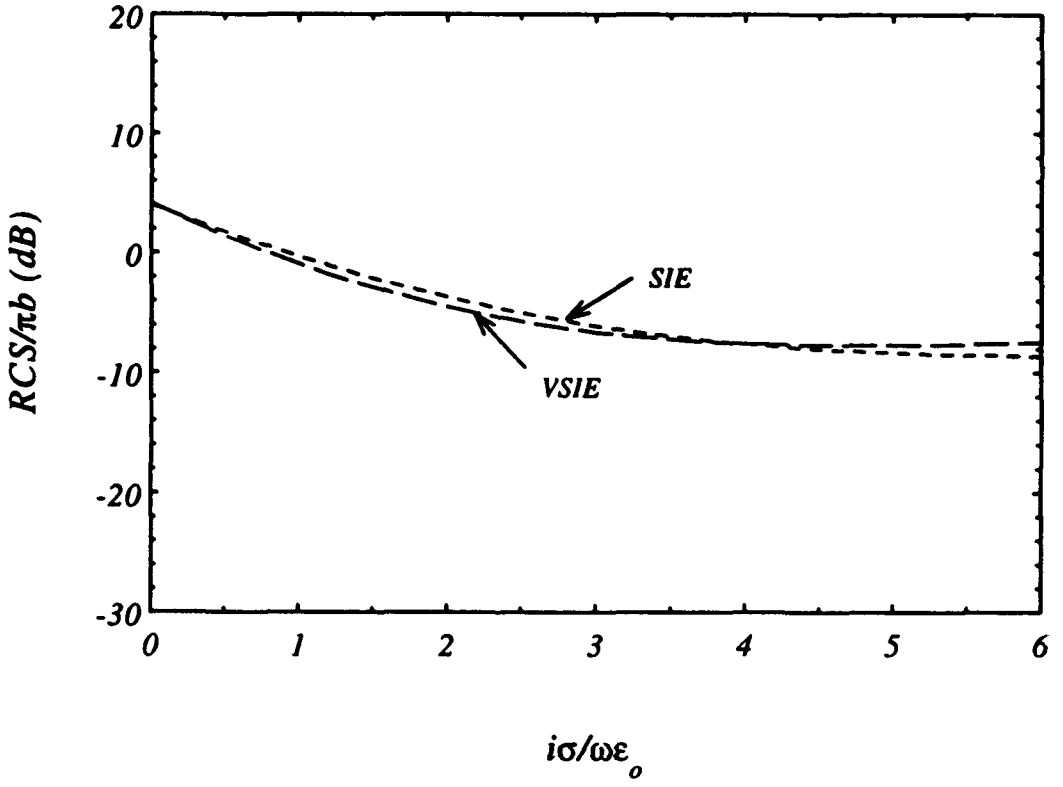

Fig. 7 Back scattering from a long dielectric square cylinder versus $(i\sigma/\omega\varepsilon_o)$, with relative permittivity $\varepsilon_r = 10$, $k_o b = 1$, $n/\lambda_d = 12$, TE polarization.

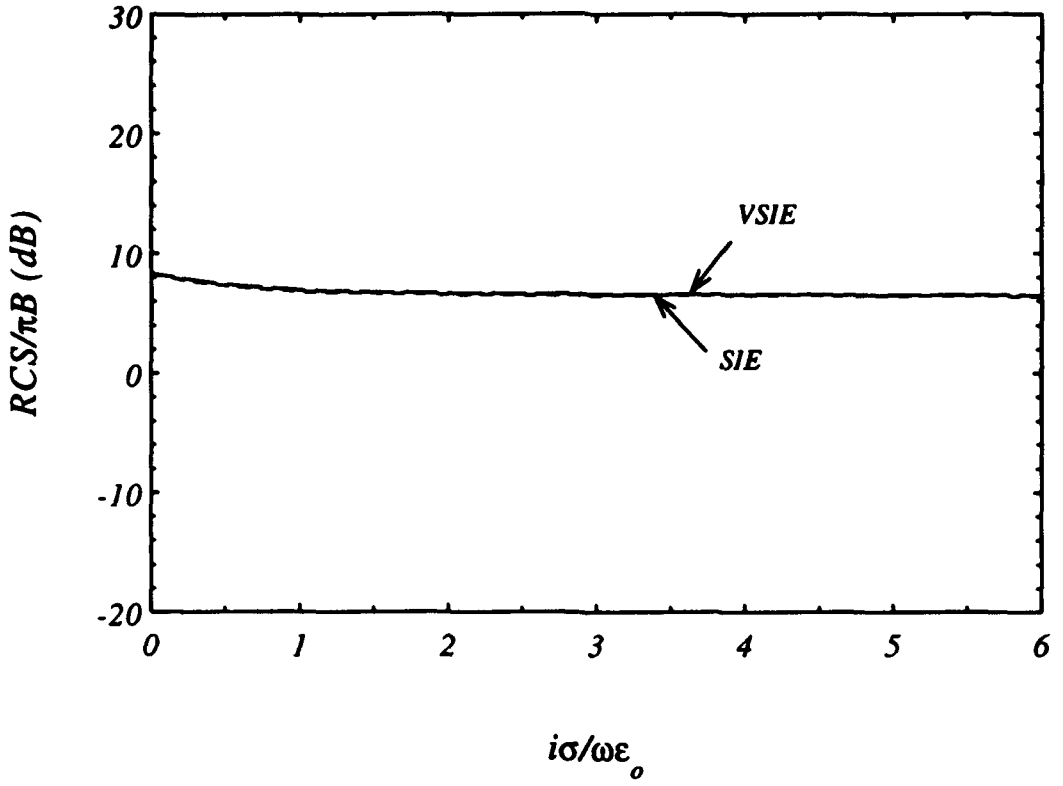

Fig. 8 Forward scattering from a long dielectric square cylinder versus $(i\sigma/\omega\varepsilon_o)$, with relative permittivity $\varepsilon_r = 10$, $k_o b = 2$, $n/\lambda_d = 12$, TE polarization.

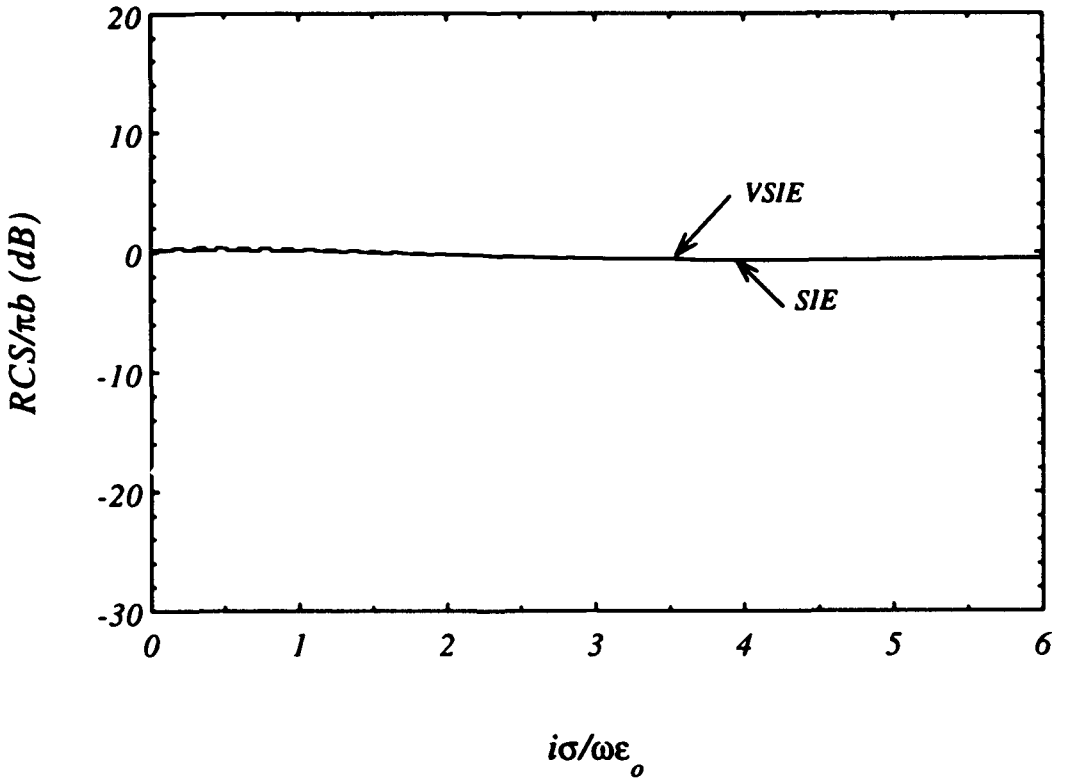

Fig. 9 Back scattering from a long dielectric square cylinder versus $(i\sigma/\omega\varepsilon_o)$, with relative permittivity $\varepsilon_r = 10$, $k_o b = 2$, $n/\lambda_d = 12$, TE polarization.

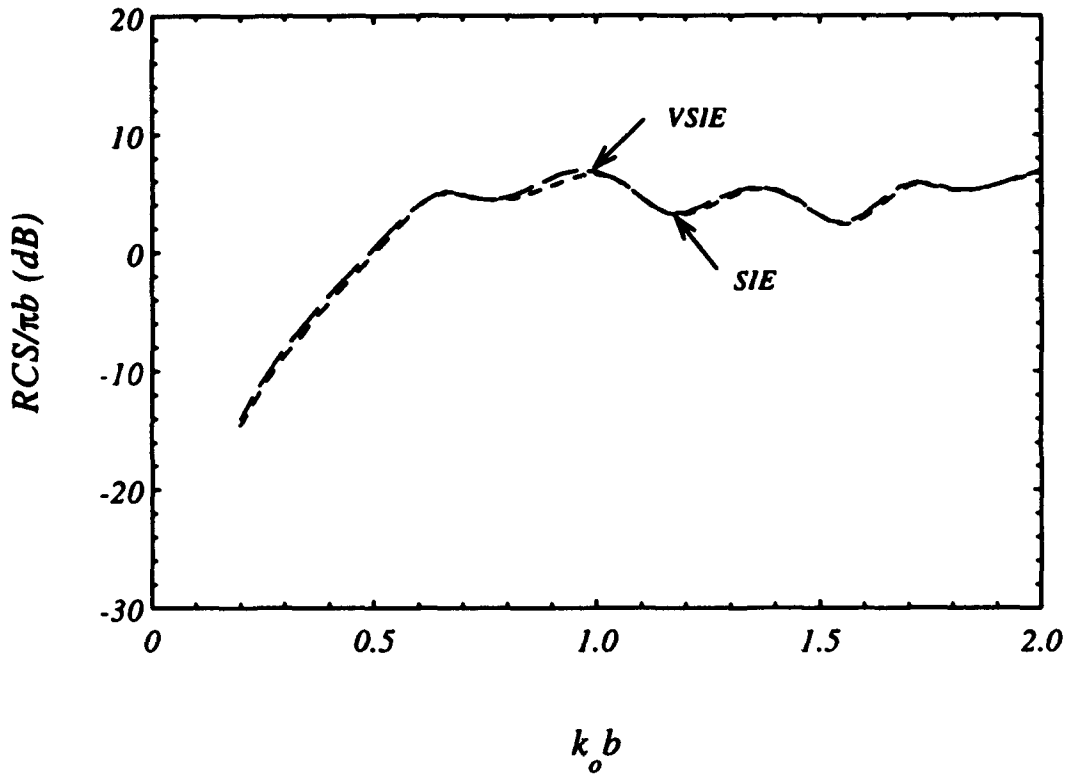

Fig. 10. Forward scattering from a long dielectric square cylinder versus $k_o b$ with relative permittivity $\varepsilon_r = 10 + i1.0$, $n/\lambda_d = 12$, TE polarization.

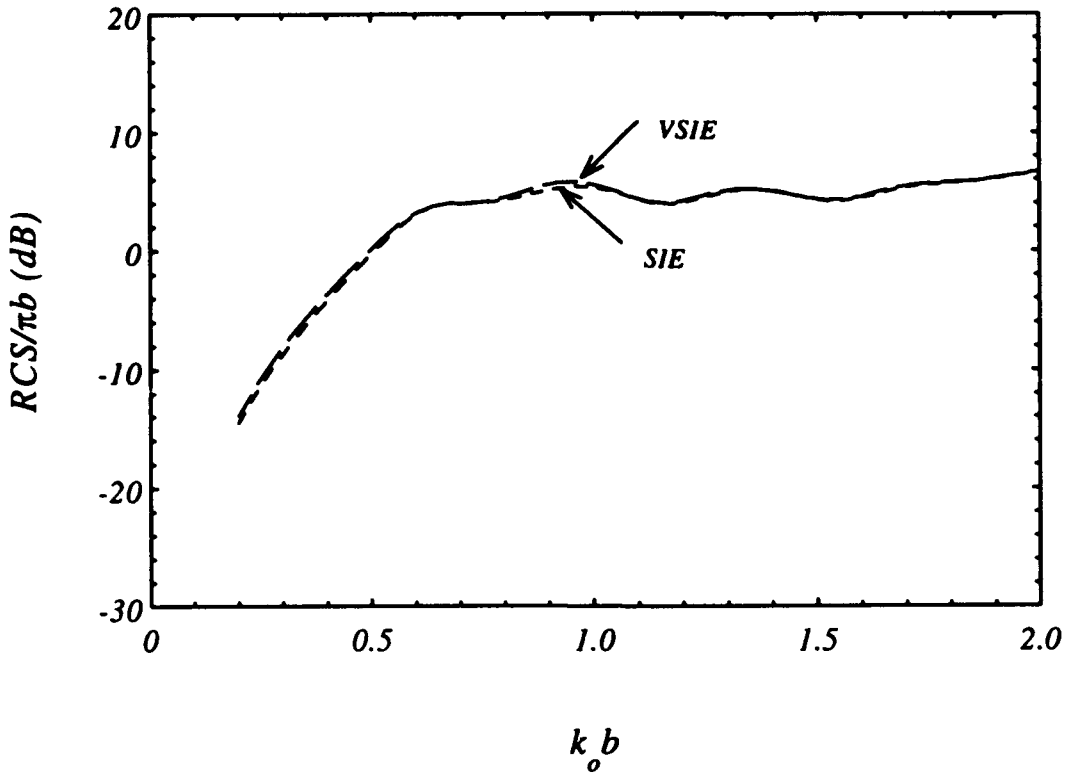

Fig. 11. Forward Scattering from a long dielectric square cylinder versus $k_o b$ with relative permittivity $\varepsilon_r = 10 + i2.0$, $n/\lambda_d = 12$, TE polarization.

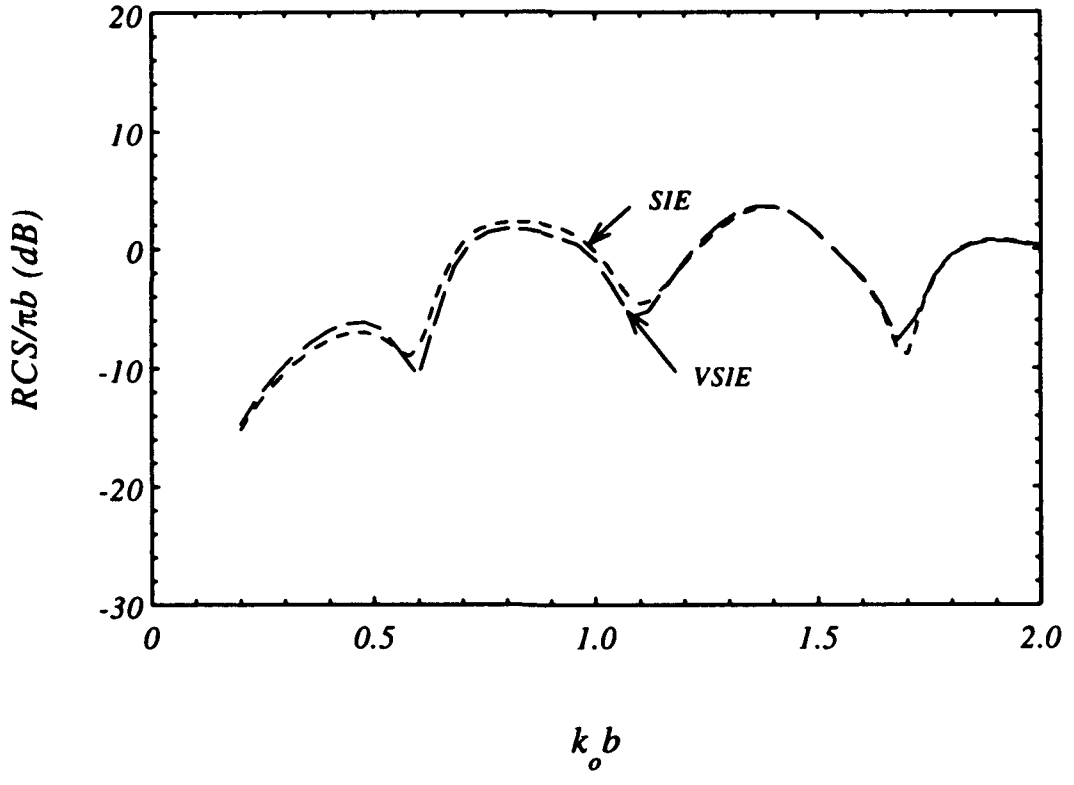

Fig. 12. Back scattering from a long dielectric square cylinder versus $k_o b$ with relative permittivity $\varepsilon_r = 10 + i1.0$, $n/\lambda_d = 12$, TE polarization.

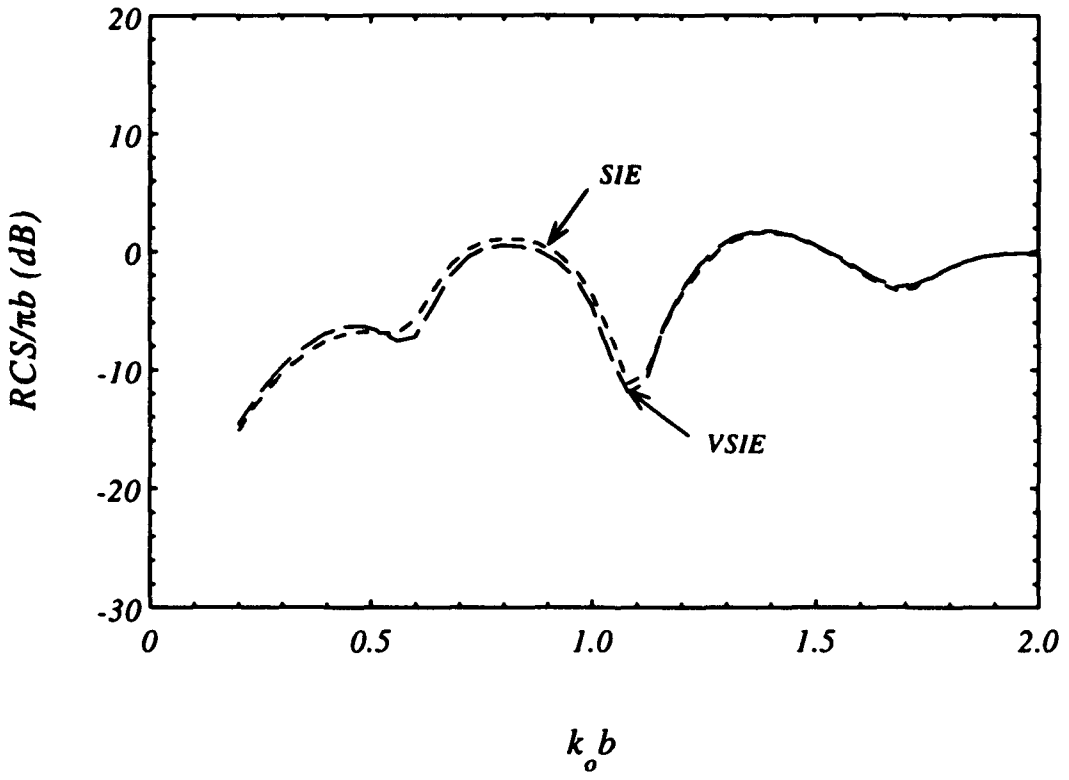

Fig. 13. Back scattering from a long dielectric square cylinder versus $k_o b$ with relative permittivity $\varepsilon_r = 10 + i2.0$, $n/\lambda_d = 12$, TE polarization.

Finally, the volume-surface integral equation and the original volume integral equation are compared with the surface integral equation for tests on dielectric square cylinders with large values ($\varepsilon_r = 72$). Referring to Fig. 14 the top two curves represent the solution from the original volume integral equation with $n/\lambda_d = 10$ and 12. It can be seen that these two curves do not correspond to the other curves. The third curve from the top of the graph represents the solution from the surface integral equation from program CICERO, and the bottom set of curves represent the solution from the volume-surface integral equation with $n/\lambda_d = 10$, 12, 20 and 35 respectively. Figure 14 shows that the solutions from the volume integral equation behave erratically, they do not at all match the solutions from the surface integral equation. The bottom curve represents the solution from the newly formulated volume-surface integral equation with $n/\lambda_d = 10$. Even though there is about a 4 dB difference at forward and back scatterer between this curve and the surface integral equation curve, with an increased number of cells the curves from the volume-surface integral equation converge to the surface integral equation curve. This is a good indication that for dielectric cylinders with large relative permittivity, the volume integral equation obviously does not work whereas the results from volume-surface integral equation clearly matches those obtained from the surface integral equation.

In order to examine why there is a still some discrepancy between the volume-surface integral and the surface integral equation method, the currents in the cylinder are examined to see if they show any unusual behavior. Figs. 15-22 represent the current densities on the cylinder versus distances along the cylinder. The relative permittivity is set to $\varepsilon_r = 72$, the size of the dielectric square cylinder is 0.30 m for TE polarization. Located exactly on the center of the dielectric square cylinder is the origin (see Fig. 15). The current density J_x versus distance on the x axis ($y = 0$) and on the y axis ($x = 0$) is plotted on Figs. 15-16. The current density J_x versus distance on the edges ($y = 0.15$ m and $x = 0.15$ m) is shown in

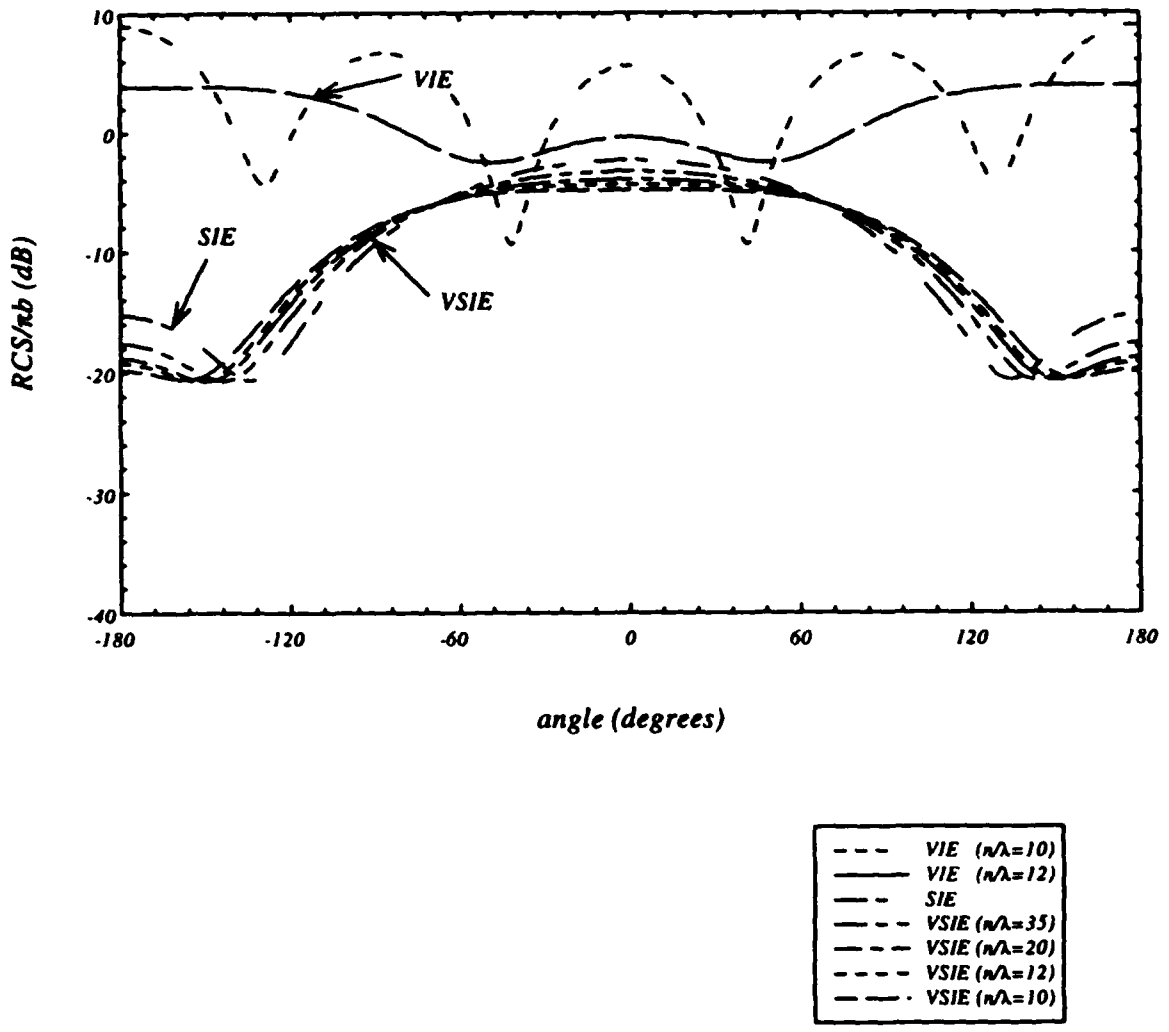

Fig. 14 Bistatic scattering from a long dielectric square cylinder versus angle, with relative permittivity $\varepsilon_r = 72$, side = 0.30 m, frequency = 100 MHz, TE polarization.

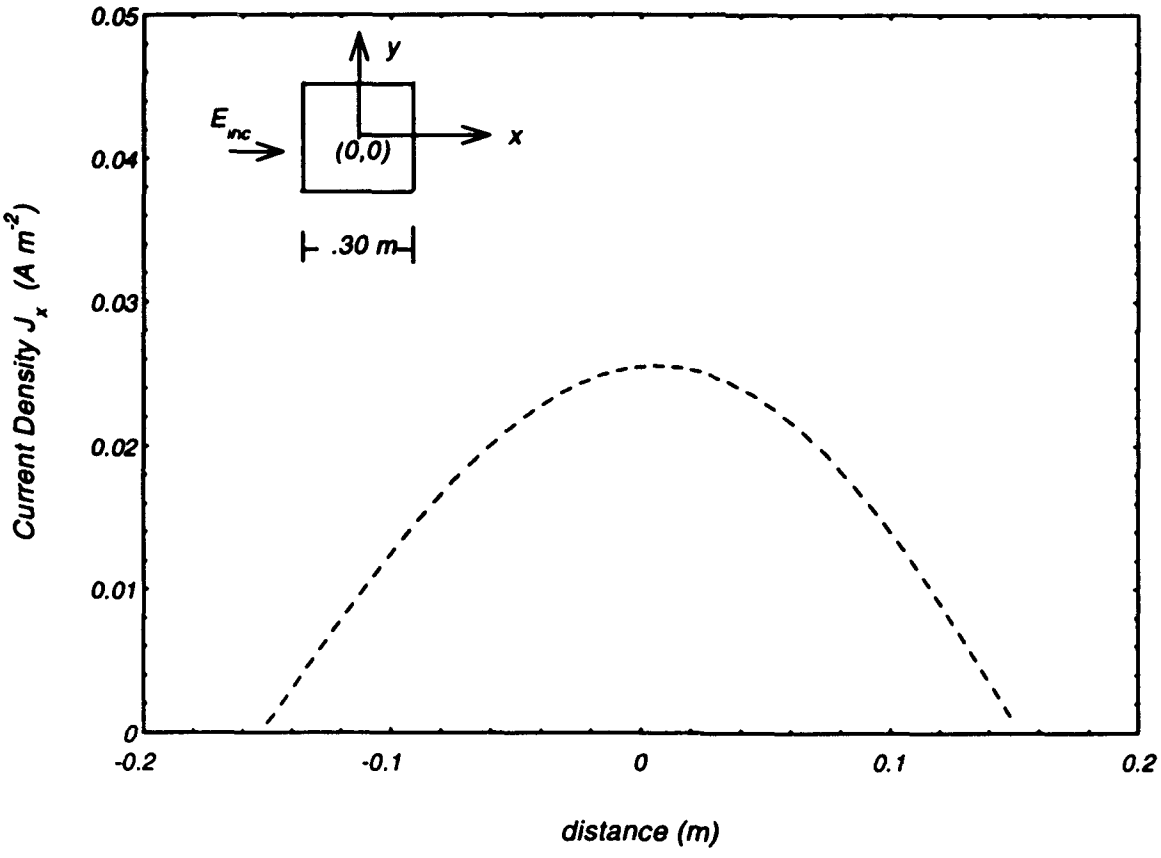

Fig. 15 Current density J_x versus distance on $y = 0$, on the dielectric square cylinder, relative permittivity $\varepsilon_r = 72$, side = 0.30 m, frequency = 100 MHz, TE polarization.

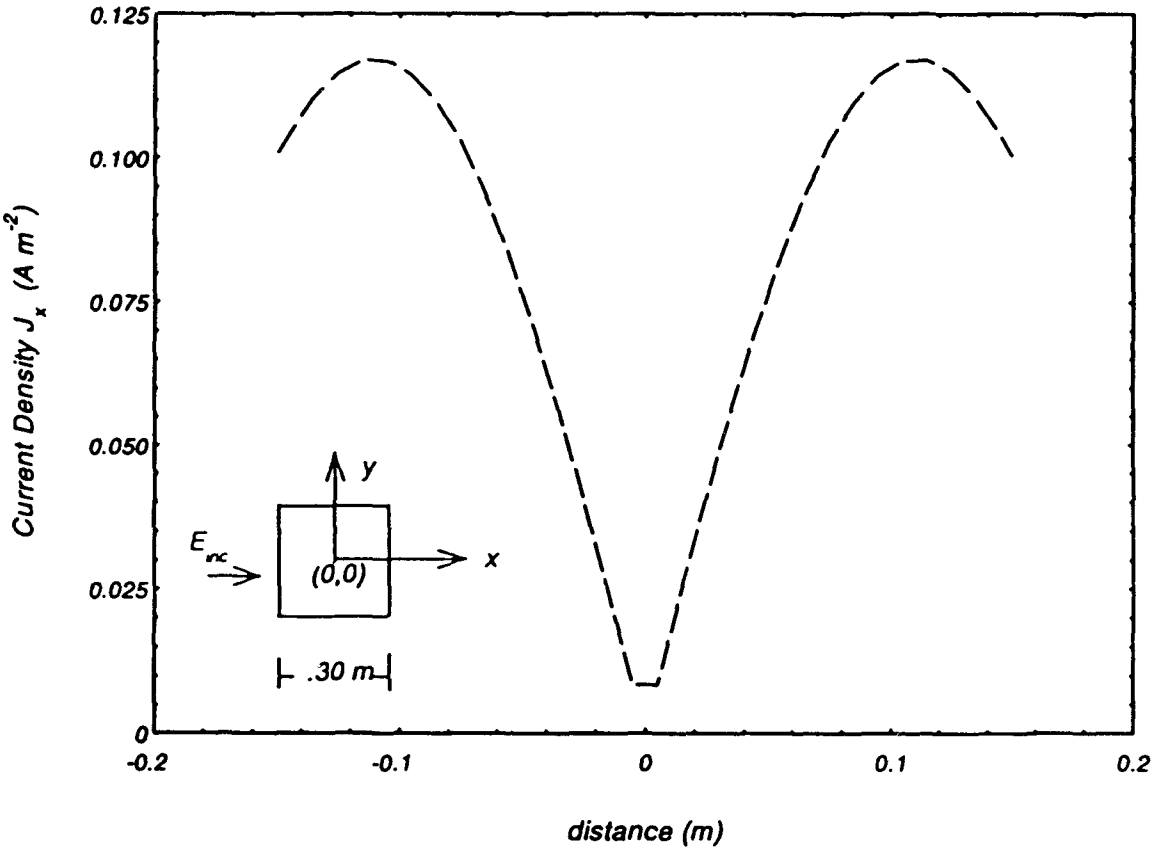

Fig. 16 Current density J_x versus distance on $x = 0$, on the dielectric square cylinder, relative permittivity $\varepsilon_r = 72$, side = 0.30 m, frequency = 100 MHz, TE polarization.

Figs. 17-18. Similarly, the current density J_y versus distance is plotted on Figs. 19-22.

The current densities on the x axis and on the y axis do not show any abnormal behavior. However, this is not the case for the current densities along the edges as illustrated in Fig. 17. The current densities experience a sudden drop at a distance of 0.125 m from the center of the cylinder. This can also be seen in Fig. 18 as well as Figs. 21-22, where the current densities either increased or decreased rapidly. The current densities close to the corner of the edges behaved exceptionally erratically [19]. Even though in our computer simulation our cell size is very small (n/λ_d is about 36), the extremely sharp jump of the currents around the edges cannot be detected unless we use an extremely fine cell size. This inadequate discretization of the edge current is the explanation of the remaining differences between the volume-surface integral equation and the surface integral equation for results of the large relative permittivity and small bodies.

Fig. 23 shows the results from a modified numerical technique: namely, we kept the same cell size constant throughout the cylinder and discretized the cell around the edges more finely in order to minimize the total number of the cells required for the computation. The bistatic scattering from the square dielectric cylinder (with relative permittivity $\varepsilon_r = 72$, TE polarization), using the volume-surface integral equation (with and without finer edge cells) is compared with the results of the surface integral equation. The number of cells per dielectric wavelength is 20. The finer discretization around the edges was made by dividing each cell adjacent to the boundary into four smaller cells (giving 40 cells per linear dielectric wavelength around the edges). Without finer discretization near the border, there is about a 2 dB average difference with the scattering computed from the surface integral equation; with finer discretization, the difference is much smaller. Specifically, Fig. 23 shows that appreciably better performance is obtained with finer discretization around the edges with 20 cells per dielectric

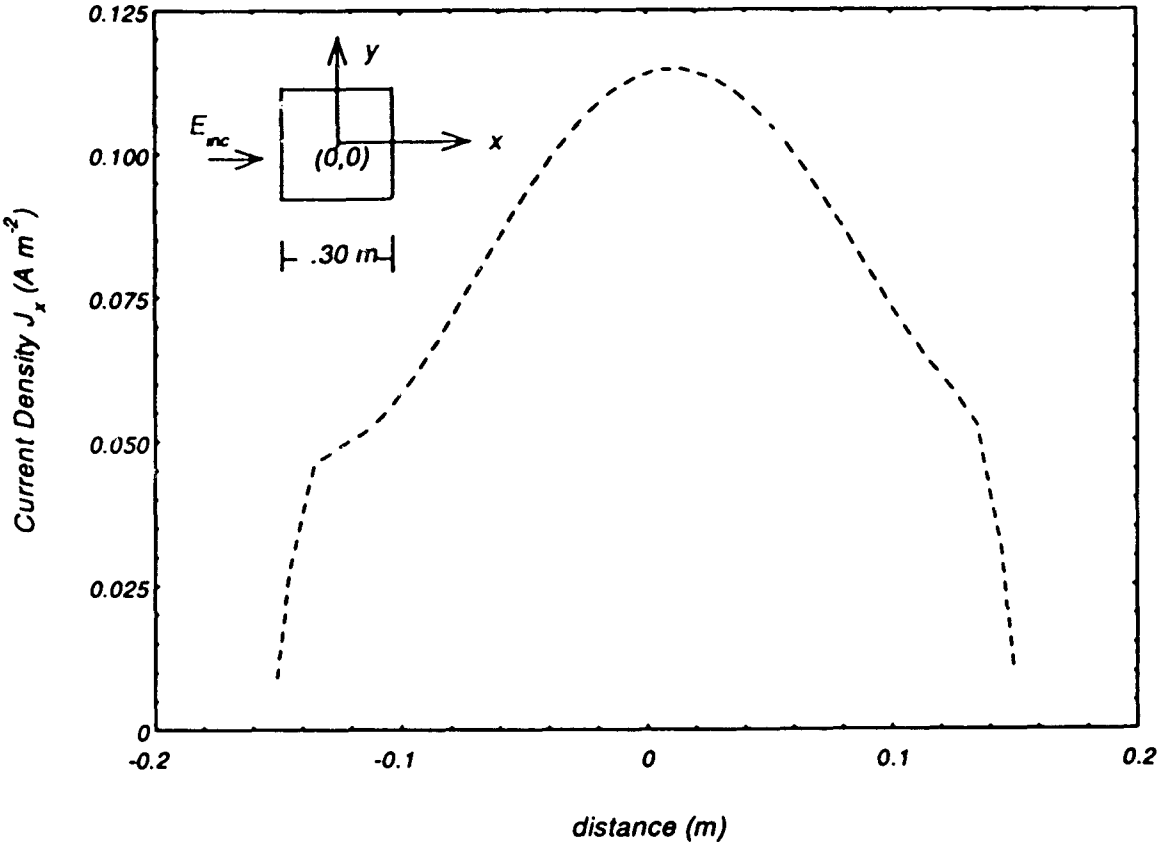

Fig. 17 Current density J_x versus distance on $y = 0.15$ m, on the dielectric square cylinder, relative permittivity $\varepsilon_r = 72$, side = 0.30 m, frequency = 100 MHz, TE polarization.

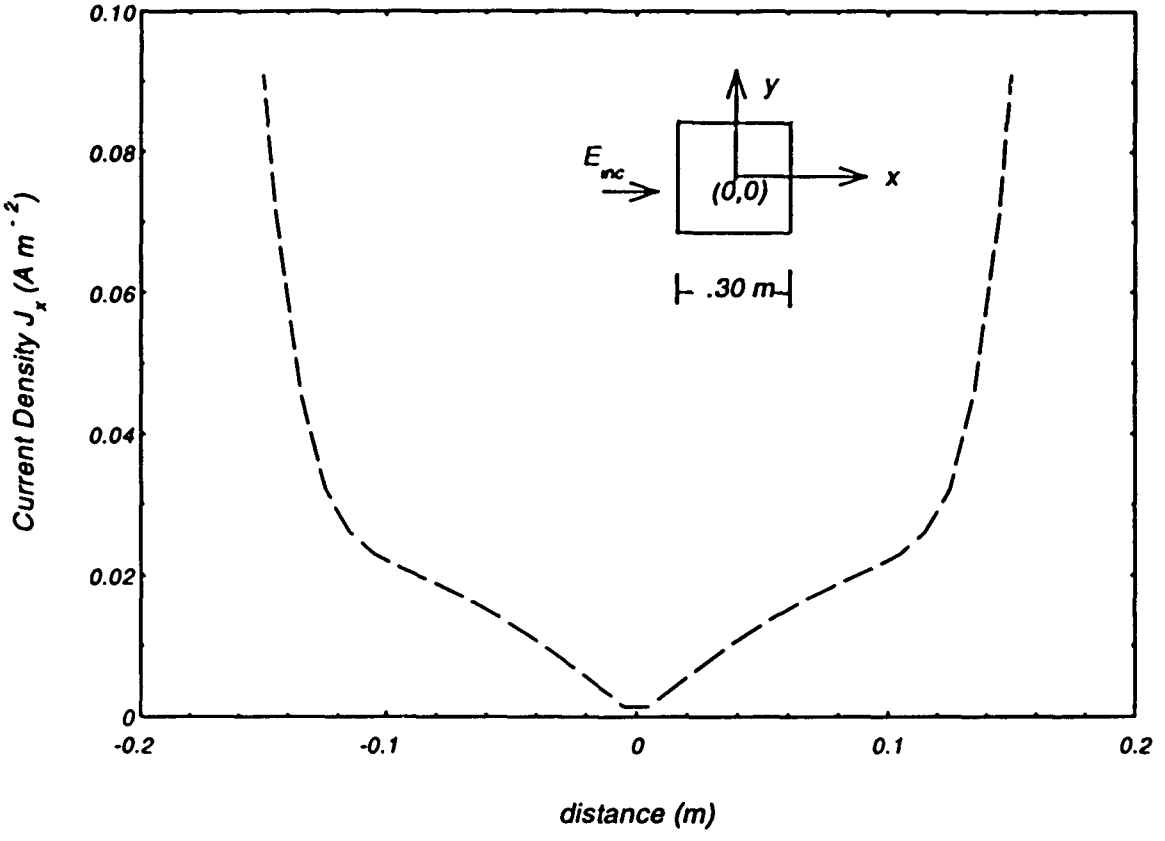

Fig. 18 Current density J_x versus distance on $x = -0.15$ m, on the dielectric square cylinder, relative permittivity $\varepsilon_r = 72$, side = 0.30 m, frequency = 100 MHz, TE polarization.

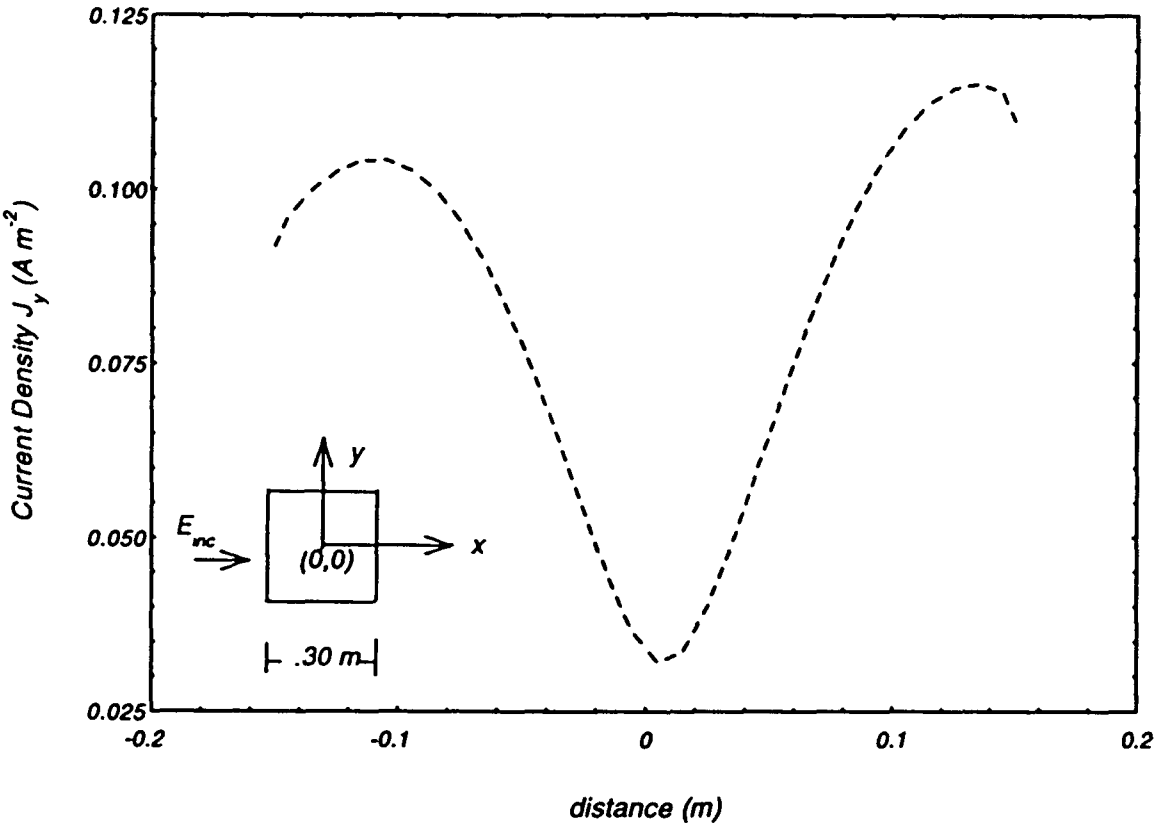

Fig. 19 Current density J_y versus distance on $y = 0$, on the dielectric square cylinder, relative permittivity $\varepsilon_r = 72$, side = 0.30 m, frequency = 100 MHz, TE polarization.

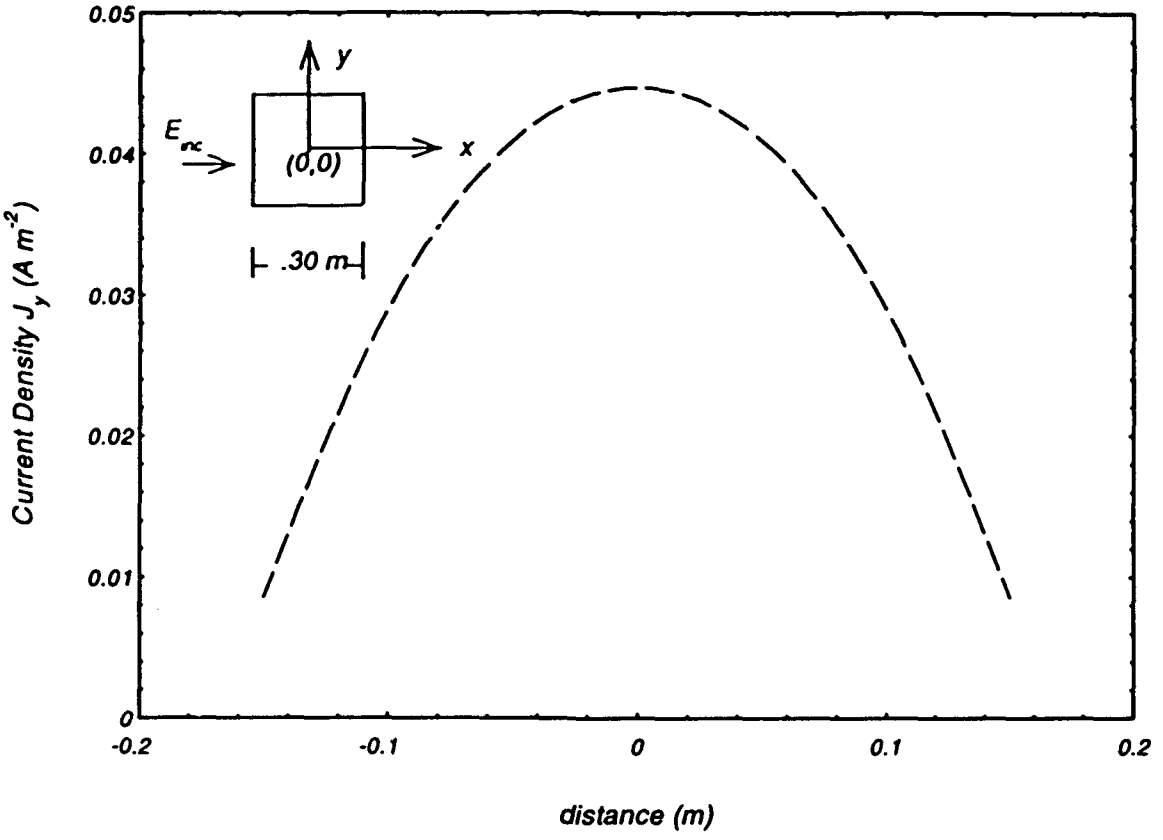

Fig. 20 Current density J_y versus distance on $x = 0$, on the dielectric square cylinder, relative permittivity $\varepsilon_r = 72$, side = 0.30 m, frequency = 100 MHz, TE polarization.

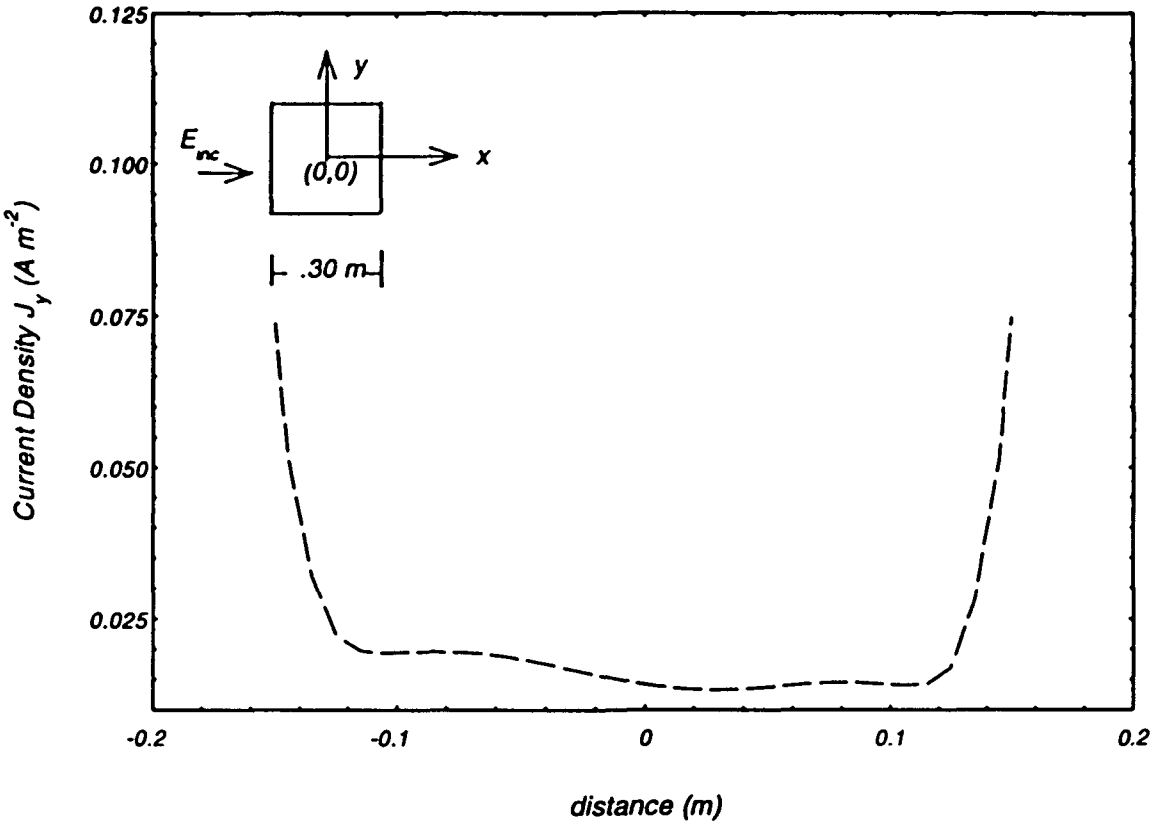

Fig. 21 Current density J_y versus distance on $y = 0.15$ m, on the dielectric square cylinder, relative permittivity $\varepsilon_r = 72$, side = 0.30 m, frequency = 100 MHz, TE polarization.

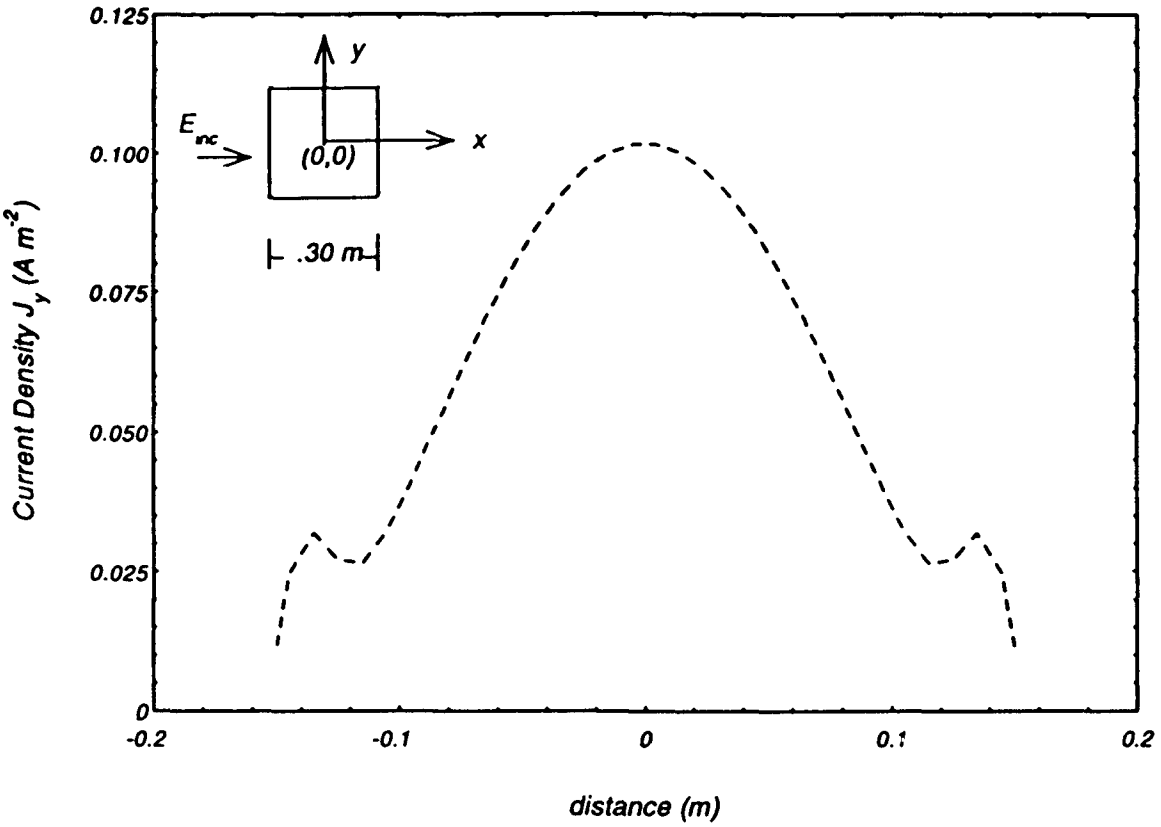

Fig. 22 Current density J_y versus distance on $x = -0.15$ m, on the dielectric square cylinder, relative permittivity $\varepsilon_r = 72$, side = 0.30 m, frequency = 100 MHz, TE polarization.

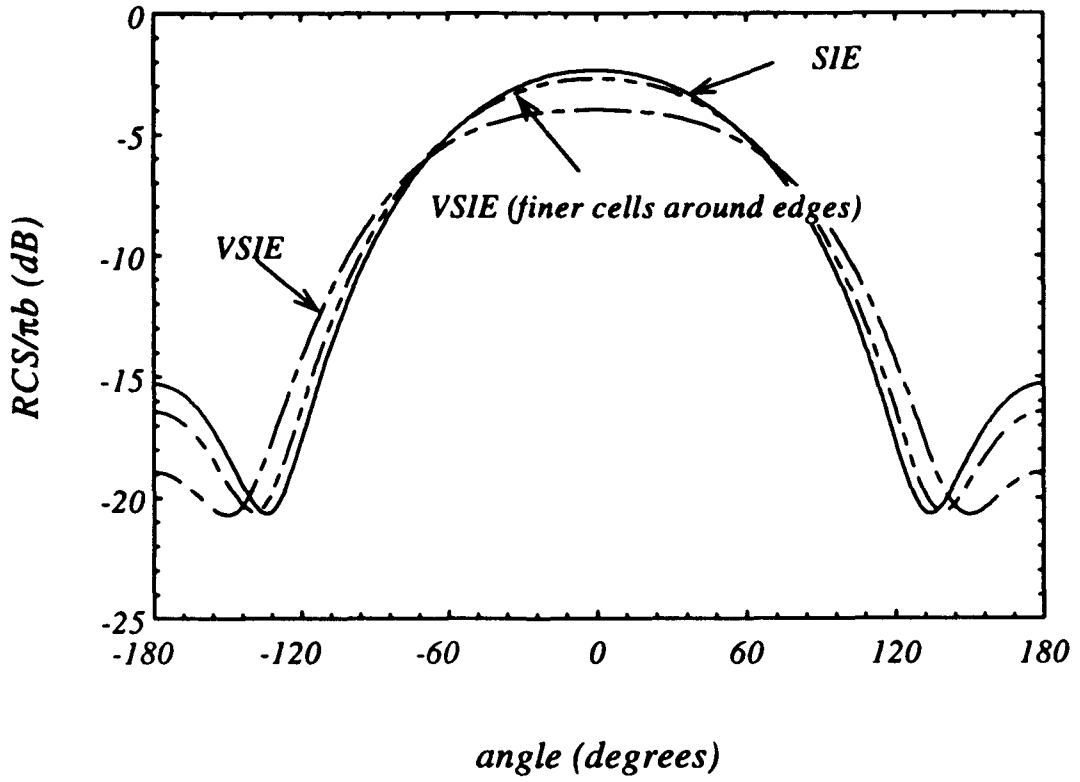

Fig. 23 Bistatic scattering from a long dielectric square cylinder dielectric square cylinder, relative permittivity $\varepsilon_r = 72$, side = 0.30 m, frequency = 100 MHz, TE polarization.

wavelength interior to the scatterer than with 36 cells per dielectric wavelength throughout.

4. CONCLUSION

In this report, a new volume-surface integral equation used to evaluate the bistatic scattering from large, high-dielectric cylinders using pulse basis functions and point matching is presented. Numerical results indicate that this new integral equation is far superior in performance to the original volume integral equation which gives highly inaccurate results with pulse basis-functions and point matching for large values of $k_o b$ as well as large relative permittivities. Finer discretization of cells along the edges significantly enhances the accuracy for small bodies with very high relative permittivities since there is a rapid change of current near the edges. This new volume-surface integral equation has been applied to 2-D scatterers, and has produced results that compared remarkably well with those of a surface integral equation. Finally, unlike previous volume-surface integral equations, it can be extended to 3-D scatterers and to obtain benchmark solutions for inhomogenous scatterers.

REFERENCES

[1] Richmond, "Scattering from a dielectric cylinder of arbitrary cross section shape," IEEE Trans. AP-13, pp. 334-341, May 1965.

[2] Richmond, "TE-wave scattering from a dielectric cylinder of arbitrary cross section shape," IEEE Trans. AP-14, pp. 460-464, July 1966.

[3] Livesay and Chen, "Electromagnetic fields induced inside arbitrarily shaped biological bodies," IEEE Trans. MTT-22, pp. 1273-1280, December 1974.

[4] Schaubert, Wilton and Glisson, "A tetrahedral modeling method for electromagnetic scattering by arbitrarily shaped inhomogeneous electric bodies," IEEE Trans. AP-32, pp. 77-85, January 1984.

[5] Cátedra, Gago and Nuño, " A numerical scheme to obtain the RCS of three-dimensional bodies of resonant size using the conjugate gradient method and the fast Fourier transform," IEEE Trans. AP-37, pp. 528-537, May 1989.

[6] Sarkar, Arvas, and Ponnapalli, "Electromagnetic scattering from dielectric bodies," IEEE Trans. AP-37, pp. 673-676, May 1989.

[7] Sarkar, "Application of conjugate Gradient method to electromagnetics and Signal Analysis," Elsevier, 1991.

[8] Yaghjian and Wang, "A conformal electric volume-surface integral equation for inhomogeneous scatterers," (paper in preparation).

[9] Jin, Liepa and Tai, "A volume-surface integral equation for electromagnetic scattering by inhomogeneous cylinders," J. Electromagnetics Waves App., vol. 2, pp. 573-588, 1988.

[10] Silberstein, "Electromagnetic scattering from dielectrics - a two-dimensional integral equation solution," RL-TR-91-115.

[11] Wang, "Volume integral equations applied to circular and square cylinders," RL-TR-92-300.

[12] Borup, Sullivan and Gandhi, "Comparison of FFT conjugate gradient method and the finite-difference time-domain method for the 2-D absorption problem," IEEE Trans. MTT-35, No. 4, pp. 383-395, April 1987.

[13] Yaghjian, "Electric dyadic Green's functions in the source region," Proceedings of the IEEE, vol. 68, pp. 248-263, February 1980.

[14] Zwamborn and van den Berg, "A weak form of the conjugate gradient FFT method for two-dimensional TE scattering problems," IEEE Trans. MTT-39, pp. 953-960, June 1991.

[15] Zwamborn, "Scattering by objects with electric contrast," Deft University Press, 1991.

[16] Wust, Nadobny, Seebass, Dohlus, John and Felix, "3-D computation of E fields by the volume-surface integral equation (VSIE) method in comparison with the finite-integration theory (FIT) method," IEEE Trans. Biomedical Engineering, vol. 40, pp. 745-759, August 1993.

[17] Yaghjian, "Augmented electric- and magnetic-field integral equations," Radio Science, vol. 16, pp. 987-1001, November-December 1981.

[18] Peterson, "Analysis of heterogeneous electromagnetic scatterers: Research progress of the past decade," Proceedings of the IEEE, vol. 79, pp. 1431-1441, October 1991.

[19] Andersen and Solodukhov, "Field behavior near a dielectric wedge," IEEE Trans. AP-26, pp. 598-602, July 1978.

[20] Joachiwocz and Pichot, "Comparison of three integral formulations for the 2-D TE scattering problem," IEEE Trans. MTT-38, pp. 178-185, February 1990.

*U.S. GOVERNMENT PRINTING OFFICE: 1994-510-117-50020

MISSION

OF

ROME LABORATORY

Mission. The mission of Rome Laboratory is to advance the science and technologies of command, control, communications and intelligence and to transition th m into systems to meet customer needs. To achieve this, Rome Lab:

a. Conducts vigorous research, development and test programs in all applicable technologies;

b. Transitions technology to current and future systems to improve operational capability, readiness, and supportability;

c. Provides a full range of technical support to Air Force Materiel Command product centers and other Air Force organizations;

d. Promotes transfer of technology to the private sector;

e. Maintains leading edge technological expertise in the areas of surveillance, communications, command and control, intelligence, reliability science, electro-magnetic technology, photonics, signal processing, and computational science.

The thrust areas of technical competence include: Surveillance, Communications, Command and Control, Intelligence, Signal Processing, Computer Science and Technology, Electromagnetic Technology, Photonics and Reliability Sciences.